

Angular-Dependent Klein Tunneling in Photonic Graphene

Zhaoyang Zhang,^{1,*} Yuan Feng¹,[†] Feng Li,^{1,†} Sergei Koniakhin,^{2,3} Changbiao Li,¹ Fu Liu¹, Yanpeng Zhang,¹ Min Xiao,^{4,5} Guillaume Malpuech^{2,‡} and Dmitry Solnyshkov^{2,6}

¹Key Laboratory for Physical Electronics and Devices of the Ministry of Education and Shaanxi Key Lab of Information Photonic Technique, School of Electronic Science and Engineering, Faculty of Electronics and Information, Xi'an Jiaotong University, Xi'an 710049, China

²Institut Pascal, PHOTON-N2, Université Clermont Auvergne, CNRS, Clermont INP, F-63000 Clermont-Ferrand, France

³Center for Theoretical Physics of Complex Systems, Institute for Basic Science (IBS), Daejeon 34126, Republic of Korea

⁴Department of Physics, University of Arkansas, Fayetteville, Arkansas 72701, USA

⁵National Laboratory of Solid State Microstructures and School of Physics, Nanjing University, Nanjing 210093, China

⁶Institut Universitaire de France (IUF), 75231 Paris, France



(Received 4 July 2022; accepted 11 October 2022; published 30 November 2022)

The Klein paradox consists in the perfect tunneling of relativistic particles through high potential barriers. It is responsible for the exceptional conductive properties of graphene. It was recently studied in atomic condensates and topological photonics and phononics. While in theory the perfect tunneling holds only for normal incidence, so far the angular dependence of the Klein tunneling and its strong variation with the barrier height were not measured experimentally. In this Letter, we capitalize on the versatility of atomic vapor cells with paraxial beam propagation and index patterning by electromagnetically induced transparency. We report the first experimental observation of perfect Klein transmission in a 2D photonic system (photonic graphene) at normal incidence and measure the angular dependence. Counterintuitively, but in agreement with the Dirac equation, we observe that the decay of the Klein transmission versus angle is suppressed by increasing the barrier height, a key result for the conductivity of graphene and its analogs.

DOI: [10.1103/PhysRevLett.129.233901](https://doi.org/10.1103/PhysRevLett.129.233901)

The Klein paradox was initially discovered in the beginning of the 20th century [1,2], immediately after the formulation of the Dirac equation. The impossibility for a relativistic electron to be confined inside the nucleus was a very important conclusion, which ultimately led to the discovery of the neutron [3]. The description of the Klein tunneling involves the quantum field theory and the concept of particles and antiparticles [2,4,5]. However, the perfect Klein tunneling with relativistic electrons has never been observed experimentally, because it requires extremely high and strongly localized energy barriers [2]. The studies of the Klein tunneling have shown a new surge of interest in the 21st century with the advent of analog systems, such as graphene [6–9], cold atoms [10], photonics [11], and even acoustic systems [12], where the Dirac Hamiltonian and the associated Klein tunneling phenomenon can be simulated on demand. The first crucial result was that the exceptional conductivity of graphene is due precisely to the Klein tunneling of the electrons in graphene making them insensitive to potential barriers associated with defects [8,13,14]. Theoretical works focused on the consequences of Klein tunneling and its limits in various 1D and 2D structures [15–17]. Further studies were focused on the *energy dependence* of the tunneling with respect to the barrier height in different systems [12].

On the other hand, the *angular dependence* of the Klein tunneling has not been studied experimentally in detail. In

graphene, ballistic electrons exhibit a broad angular distribution, smoothing out the dependence [18]. Analog systems potentially offer a better control over parameters. However, the experiments on Klein tunneling were mostly implemented in 1D structures which only allow us to study the normal incidence case [10,11]. Theoretically, in 2D systems, the tunneling is expected to be perfect only for normal incidence, and should quickly drop with the incident angle, depending on the particle energy and on the barrier height [8,19]. In 2D materials, Klein tunneling is at the basis of recent experiments and proposals in “electron optics” [20], such as negative refraction [18] (also in acoustics [21]), Veselago lens [22–24], Klein collimation [25], and 2D microscopes [26].

The rules of the angular dependence, being an indispensable addition to the Klein tunneling theory, show exceptional properties compared to ordinary reflecting rules, and are therefore crucial both from the fundamental point of view, and for the applied properties of graphene, [8,27–29], 2D materials [30,31], and their optical analogs, as the incidence is rarely perfectly normal in realistic situations.

The possibilities to study Klein tunneling in 2D photonic systems were proposed in previous theoretical works using photonic graphene [32]. Photonic graphene has recently emerged as a promising analog system with various implementations [33–37]. It is based on the propagation of a light probe beam in a 2D honeycomb lattice of

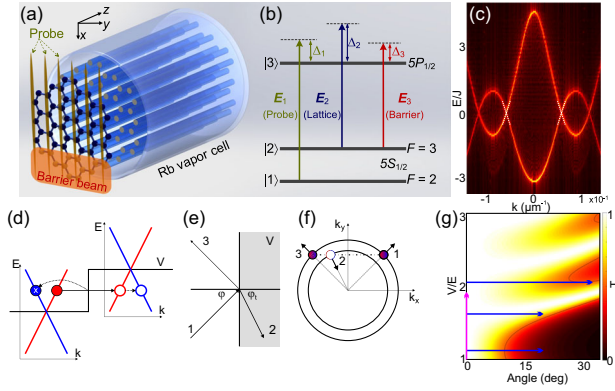


FIG. 1. Photonic graphene and Klein tunneling. (a) A honeycomb lattice is induced in the Rb vapor cell by the interference of three coupling beams E_2 , E'_2 , and E''_2 . The probe field is close either to the Dirac (formed by the interference of E_1 and E'_1) or Γ point (only Gaussian E_1). The potential barrier is formed by another stripe-shaped coupling beam E_3 . The refractive index experienced by the probe beam is governed by the EIT effects arising from both the hexagonal and stripe fields. (b) The Rb atomic energy levels and the configuration of the EIT effect. (c) Calculated dispersion of photonic graphene; white dashed lines are the regions described by the Dirac Hamiltonian in Eq. (1). (d)–(f) Scheme of the Klein tunneling: filled circles—particle states, empty circles—hole states. (d) Perfect Klein tunneling in one dimension. The colors of lines of the dispersion $[E(k)]$ and circles (states) correspond to the conserved particle-hole pseudospin. Crosses mark the forbidden final states. V is the potential. (e) Klein tunneling in two dimensions (real space, x - y plane), arrows indicate the group velocity, $\varphi = \tan^{-1}(k_y/k_x)$. (f) States in the 2D reciprocal space. k_y is conserved. Arrows mark the group velocity. All transitions are allowed, because the states are not orthogonal. (g) Transmission through a finite barrier calculated with Eq. (2) as a function of the incidence angle and the barrier height. Magenta and blue arrows: experimental scans (Figs. 2 and 3).

refractive index. The evolution of the probe beam is well described by the paraxial approximation of Maxwell's equations, where the propagation along an axis is mapped to an effective time (see Ref. [38]). This configuration allows one to emulate various Hamiltonians, including the one of graphene [39]. The advantage of optical systems is the possibility of direct observation of the wave functions, instead of the integral quantities used in solid state physics, such as conductivity. For example, in topological photonics it has allowed the observation of the photonic quantum Hall [34,40–42] and quantum spin or valley Hall effects [43–49], with the associated chiral edge states, promising for applications. Recently, reconfigurable photonic graphene in atomic vapor cells has allowed us to study the dynamics of singularities (quantum vortices) appearing in the Dirac equation [50]. Obviously, the implementation of angular dependent Klein tunneling in the photonic graphene requires a proper experimental strategy to allow building potential boundaries between areas of linear dispersion.

In this Letter, we use the photonic graphene implemented in an atomic vapor cell to study the angular and barrier height dependence of the Klein tunneling, in which the potential boundary is established via the effect of electromagnetically induced transparency (EIT). Our measurements are in excellent agreement with the analytical theory based on the Dirac equation. We observe a perfect tunneling for normal incidence and a strong decrease of the transmission versus the incidence angle. This angular dependence is much weaker if the barrier height is increased. This never observed counterintuitive behavior is probably responsible for the high conductivity of electronic graphene, where scattering defects typically correspond to large potential barriers.

To study the Klein tunneling and its peculiar angular dependence, we used a highly reconfigurable implementation of photonic graphene based on EIT in atomic vapors [50–52]. EIT typically occurs in a three-level atomic system driven by a strong coupling field that modulates the refractive index of the sample. The scheme of the experimental setup is shown in Fig. 1(a). Three vertically polarized coupling beams E_2 , E'_2 , and E''_2 (the lattice beams) from the same external-cavity diode laser propagate along z with a small angle $\sim 0.5^\circ$ between each other, forming a hexagonal interference pattern in the x - y plane. The photonic graphene with a lattice constant $a \approx 60 \mu\text{m}$ is formed by the dark lattice sites with higher refractive index (inversely related to the intensity of the coupling field under the EIT condition, see Ref. [38]), as determined by the chosen two-photon detuning [Fig. 1(b)]. Formed by the interference of the coupling beams, the honeycomb pattern stays approximately uniform along z throughout the entire length of the atomic cell. A narrow, line-shaped beam E_3 (the barrier beam, from a second laser) parallel to the z axis serves as a static potential barrier (see Ref. [38]). This barrier is located within the honeycomb lattice potential, as shown in Fig. 1(a), sufficiently close to the center to avoid the effects of the lattice contrast reduction. The dispersion of the photonic graphene, calculated in the paraxial approximation [38], is shown in Fig. 1(c). The white dashed lines indicate the regions described by the Dirac Hamiltonian (see below). The probe beam or beams are sent at an angle with the z axis, controlling their wave vector in the x - y plane (see Fig. S2 [38], showing the spatial arrangement of all beams). Their size and position at the entrance of the vapor cell are also controlled, determining the wavepacket in real space. To probe the Γ point, the beam is sent close to the z axis. To excite the Dirac points, the probe beam is split into two beams E_1 and E'_1 , whose angle with z axis is close to the Dirac point. They form an interference pattern controlling the pseudospin at the Dirac points [50]. The probe feels the combined modulation of susceptibility imposed by the EIT effects of both the lattice and the barrier beams. To observe the Klein tunneling, the probe beams are moved slightly away from the Dirac point

by fine-adjusting the beam angle. The probe beams interact with the honeycomb lattice and the barrier, while all of them are propagating along z through the atomic vapor cell. The 2D dynamics of Klein tunneling occurs within the x - y plane, and the z axis is regarded as the effective axis of time (see Ref. [38]). Similarly, we can send a single probe beam close to the Γ point for comparison.

The Klein tunneling is best known in the case of a massless Dirac Hamiltonian for ultrarelativistic particles. The model system for the study of the angular dependence of the tunneling should be at least two-dimensional. The corresponding Hamiltonian reads

$$\hat{H} = c\boldsymbol{\sigma} \cdot \hat{\mathbf{p}}, \quad (1)$$

where $\hat{\mathbf{p}}$ is a two-dimensional momentum operator and $\boldsymbol{\sigma}$ is a vector of Pauli matrices. This effective Hamiltonian is implemented at the corners of the Brillouin zone in honeycomb lattices [7]. The corresponding eigenstates are characterized by a linear dispersion of eigenenergies $E = \pm\hbar c|k|$ and a particle-antiparticle spinor for eigenstates $(\pm e^{-i\varphi}, 1)^T/\sqrt{2}$, where φ is the polar angle of the wave vector \mathbf{k} . The perfect Klein tunneling under normal incidence is due to the conservation of this pseudospin and to the particle-hole conversion, making possible the propagation at negative energies. This is illustrated in Fig. 1(d), showing the normal incidence case with the dispersion branches in two regions characterized by potentials 0 and V . The color of the branches indicates the configuration of the spinor $(-1, 1)^T/\sqrt{2}$ (red) and $(1, 1)^T/\sqrt{2}$ (blue). At the barrier, the incident particle is converted into a hole with a negative energy, which continues to propagate in the same direction because it has the same group velocity. Backscattering (from “red” to “blue” states) is impossible because of the pseudospin conservation.

In two dimensions, for an arbitrary angle of incidence, the spinors of the branches involved in the scattering are not orthogonal anymore, and the reflection becomes allowed. It is illustrated in Fig. 1(e). The angle of incidence φ is defined by the orientation of velocity of the incident beam with respect to the barrier. The angle of transmission φ_t is described by an analog of the Snell-Descartes law, $E \sin \varphi = -(E - V) \sin \varphi_t$. It can be either higher or lower than the angle of incidence, depending on the barrier height V with respect to the particle energy E . The scheme of the process in the reciprocal space is shown in Figs. 1(e) and 1(f): the wave vector along the interface k_y is conserved. For $E > V$, the isoenergetic circle for the holes is smaller. In this case, the transmission at high angles becomes completely impossible and the reflection is total. For a barrier of a finite length d , the transmission can be found analytically as [19]

$$T = \frac{\cos^2 \varphi \cos^2 \varphi_t}{\cos^2 \varphi \cos^2 \varphi_t \cos^2(k'_x d) + \sin^2(k'_x d) (1 + \sin \varphi_t \sin \varphi)^2}, \quad (2)$$

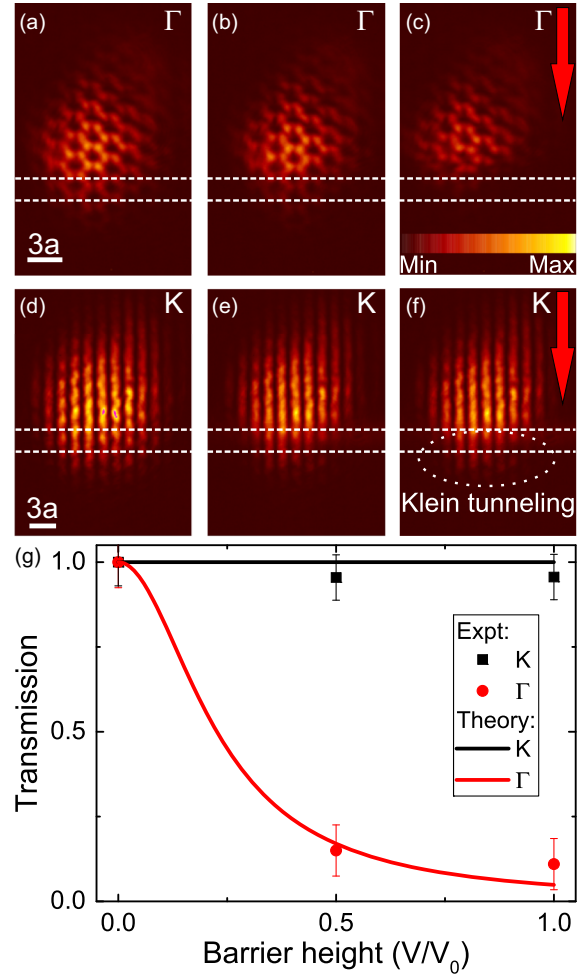


FIG. 2. Klein tunneling at normal incidence. The barrier is delimited by white dashed lines. The probe motion (group velocity) is indicated by the red arrows. (a)–(c) Ordinary quantum-mechanical tunneling close to the Γ point excited by a single Gaussian probe beam. (d)–(f) Klein tunneling excited by the interference of two probe beams. The high transmission region is highlighted by a dashed ellipse. The barrier height increases from zero (a),(d) to maximum $V_0 = 1.9E$ (c),(f). (g) Transmission for both cases (dots—experiment, lines—theory) for K and Γ points. Error bars mark the experimental uncertainty. White bars in (a),(d) show the scale.

where $k'_x d = -2\pi l \sqrt{1 - 2\epsilon + \epsilon^2 \cos^2 \varphi}$, $l = Vd/(2\pi\hbar c)$, $\epsilon = E/V$. This expression exhibits a strong angular and barrier height dependence. The angular dependence is maximal when $V/E \rightarrow 1$, where only a narrow range of incident angles lead to transmission, with total external reflection at higher angles. This transmission is shown in Fig. 1(g) as a function of the angle of incidence and the barrier height. In the following, we present the experimental scans of this dependence along the arrows (magenta and blue) shown in this panel.

First, we show the experimental results confirming the existence of the Klein tunneling at normal incidence [magenta arrow in Fig. 1(g)], comparing it with the case

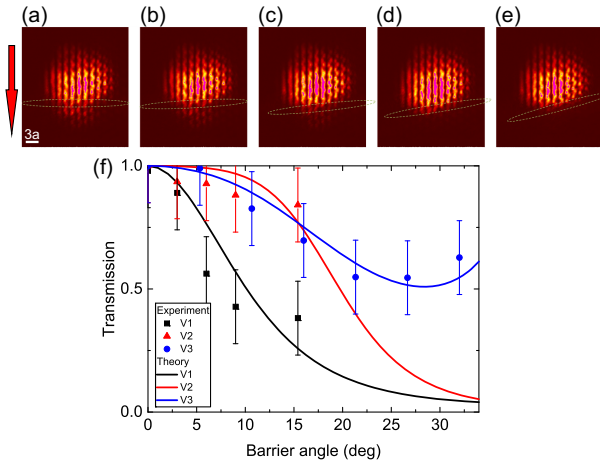


FIG. 3. Angular and barrier height-dependent Klein tunneling. The barrier is marked with a dashed ellipse. The probe propagation is marked by the red arrow. (a)–(e) Experimental images of the probe intensity after the cell with barrier rotation angles 0° , 3° , 6° , 9° , and 15° , respectively, for barrier height V_1 . (f) Angular dependence of the transmission for two barrier heights (V_1 , black; V_2 , red; V_3 , blue; $V_1 < V_2 < V_3$): dots, experiment; lines, theory. The error bars mark the experimental uncertainty. V_1 , V_2 , and V_3 correspond to detunings $\Delta_3 = -90$, -110 , and -115 MHz, respectively. White bar in (a) shows the scale.

of massive nonrelativistic particles as a reference. The large size of the wave packet in real space ensures its strong focusing in reciprocal space. The lattice and the barrier intensity do not appear in the experimental Figs. 2 and 3, measured at the probe frequency. The lattice covers the whole image, and the position of the barrier is indicated with dashed lines.

Figure 2 shows the experimental images of ordinary quantum-mechanical tunneling [Figs. 2(a)–2(c)], achieved close to the Γ point in photonic graphene [38]. The barrier height is increased from left to right from zero [panels (a), (d)] to maximum [panels (c), (f)] by experimentally changing the frequency detuning of the barrier beam, and the transmitted intensity clearly decreases. For the case of Klein tunneling, achieved with a wave packet close to the K point (with velocity towards the barrier) described by the Dirac Hamiltonian in Eq. (1), the increase of the barrier height does not lead to obvious decrease of the tunneling [panels (d)–(f)]. Even for the highest barrier [$V = V_0$, panel (f), see Ref. [38]], intensity can still be observed inside and beyond the barrier region (marked “Klein tunneling” in the figure). This is summarized in Fig. 2(g), showing the relative transmission with zero-barrier baseline (see Ref. [38]) as a function of the barrier height in both cases, as well as the theoretical predictions. In the case of Klein tunneling (probe close to the K point), a full transmission $T = 1$, independent of the barrier height V is expected theoretically (black solid line). This is indeed confirmed by the experiment (black squares). This full transmission is in striking contrast with the behavior of the

wave packets close to the Γ point, whose transmission exhibits a rapid decrease with the barrier height in experiments (red circles). This case is well described by the usual quantum-mechanical tunneling formula for massive particles [38,53] (red solid line).

Finally, we demonstrate the strong angular dependence of the Klein tunneling (Fig. 3) for weak barrier height, the suppression of this dependence when the barrier becomes higher, and the recovery of transmission at higher angles for even higher barrier heights [three blue arrows in Fig. 1(g)]. Figures 3(a)–3(e) show experimental images of the wave packet with varying angle of the barrier potential (from 0° to $\sim 15^\circ$ for the first two scans and from 0° to 32° for the third one) with respect to the probe wave vector. The angle of incidence is therefore controlled by the rotation of the barrier (“sample”), as in the $\theta - 2\theta$ goniometer configuration in x-ray diffraction, for example. The beam is still propagating along x (lying in the x - z plane), but the barrier is not perpendicular to this direction any more. The experimentally measured transmission is plotted in Fig. 3(f) as black squares, red triangles, and blue circles. The three sets of data correspond to different barrier heights $V_1 \approx 1.1E$, $V_2 \approx 1.7E$, and $V_3 \approx 2.05E$ (see Ref. [38]). Theoretical estimates, calculated using Eq. (2) neglecting the barrier ellipticity, are shown as solid lines of the corresponding color. The good agreement of the experiment and the theory in Fig. 3 confirms the validity of the description of graphene-like structures in terms of the Dirac Hamiltonian. The fact that the perfect tunneling is observed at zero incidence for three different barrier heights proves that the effect in question is not resonant tunneling [54], but really Klein tunneling. It is also possible to refute the hypothesis of resonant tunneling for ordinary quantum-mechanical particles, because it does not exist for energies below the barrier (for one single barrier), where there is no real wave vector.

Overall, a higher tunneling is observed at all angles for a higher barrier $V_2 > V_1$. A smaller barrier exhibits a faster decrease of the tunneling with φ . This counterintuitive behavior can be understood qualitatively from the modified Snell-Descartes law illustrated by Fig. 1(f): reducing the barrier height reduces the transmitted wave vector and extends the total external reflection region for $V/2 < E < V$. Thus, the Klein tunneling is paradoxical not only in its perfectness, but also in its rapid decay with incidence angle for small barriers. Thus, smaller defects can strongly affect the transport properties. For larger barrier heights, the recovery of transmission can be expected at higher angles due to the finite barrier thickness [19] (similar to interference fringes). This is confirmed by the third measurement V_3 , where we have accessed higher angles, and where the transmission $T(\varphi)$ starts to increase after passing through a minimum.

To conclude, we have used an implementation of photonic graphene based on EIT to measure one of the key features of the Klein tunneling—its strong and

counterintuitive angular dependence. Our Letter makes an important step towards the potential applications of the relativistic particle-hole physics of graphenelike structures. We have been able to measure the angular dependence up to the incidence angle of 32° . The atomic vapor cells in the regime of EIT have the important advantage of the possibility to reconfigure the system on-demand. The use of Klein tunneling in future photonic devices [55] might require further miniaturization of the system. The key parameter determining the size of the system, the lattice constant, can be reduced from $60\ \mu\text{m}$ down to a few microns by the use of patterned microcavities [56,57], which also offer the possibilities of potential engineering and have a large potential for photonic applications [58]. Practical applications will also require the knowledge of the limitations of the approximations of the theoretical model, for example, for particularly narrow barriers. Angular dependence of Klein tunneling should also be measurable in such systems [32], and experiments in this direction have already begun [59].

This work was supported by National Key R&D Program of China (2018YFA0307500, 2017YFA0303703), the Key Scientific and Technological Innovation Team of Shaanxi Province (2021TD-56), National Natural Science Foundation of China (12074303, 62022066, 12074306, 11804267). We acknowledge the support of the EU “TOPOLIGHT” project (964770), of the ANR Labex Ganex (ANR-11-LABX-0014), and of the ANR program “Investissements d’Avenir” through the IDEX-ISITE initiative 16-IDEX-0001 (CAP 20-25). S. K. was supported by the Institute for Basic Science in Korea, Young Scientist Fellowship (IBS-R024-Y3-2021).

*zhyzhang@xjtu.edu.cn

†felix831204@xjtu.edu.cn

*guillaume.malpuech@uca.fr

- [1] O. Klein, *Zeitschrift für Physik* **53**, 157 (1929).
- [2] W. Greiner, B. Mueller, and J. Rafelski, *Quantum Electrodynamics of Strong Fields* (Springer, Berlin, 1985).
- [3] J. Chadwick, *Nature (London)* **129**, 312 (1932).
- [4] N. Dombey and A. Calogeracos, *Phys. Rep.* **315**, 41 (1999).
- [5] P. Krekora, Q. Su, and R. Grobe, *Phys. Rev. Lett.* **92**, 040406 (2004).
- [6] P. R. Wallace, *Phys. Rev.* **71**, 622 (1947).
- [7] G. W. Semenoff, *Phys. Rev. Lett.* **53**, 2449 (1984).
- [8] M. I. Katsnelson, K. S. Novoselov, and A. K. Geim, *Nat. Phys.* **2**, 620 (2006).
- [9] S. Das Sarma, S. Adam, E. H. Hwang, and E. Rossi, *Rev. Mod. Phys.* **83**, 407 (2011).
- [10] T. Salger, C. Grossert, S. Kling, and M. Weitz, *Phys. Rev. Lett.* **107**, 240401 (2011).
- [11] F. Dreisow, R. Keil, A. Tnnermann, S. Nolte, S. Longhi, and A. Szameit, *Europhys. Lett.* **97**, 10008 (2012).
- [12] X. Jiang, C. Shi, Z. Li, S. Wang, Y. Wang, S. Yang, S. G. Louie, and X. Zhang, *Science* **370**, 1447 (2020).
- [13] B. Huard, J. A. Sulpizio, N. Stander, K. Todd, B. Yang, and D. Goldhaber-Gordon, *Phys. Rev. Lett.* **98**, 236803 (2007).
- [14] N. Stander, B. Huard, and D. Goldhaber-Gordon, *Phys. Rev. Lett.* **102**, 026807 (2009).
- [15] J. Otterbach, R. G. Unanyan, and M. Fleischhauer, *Phys. Rev. Lett.* **102**, 063602 (2009).
- [16] S. Longhi, *Phys. Rev. B* **81**, 075102 (2010).
- [17] O. Bahat-Treidel, O. Peleg, M. Grobman, N. Shapira, M. Segev, and T. Pereg-Barnea, *Phys. Rev. Lett.* **104**, 063901 (2010).
- [18] G.-H. Lee, G.-H. Park, and H.-J. Lee, *Nat. Phys.* **11**, 925 (2015).
- [19] P. E. Allain and J. N. Fuchs, *Eur. Phys. J. B* **83**, 301 (2011).
- [20] S. Chen, Z. Han, M. M. Elahi, K. M. Habib, L. Wang, B. Wen, Y. Gao, T. Taniguchi, K. Watanabe, J. Hone *et al.*, *Science* **353**, 1522 (2016).
- [21] H. He, C. Qiu, L. Ye, X. Cai, X. Fan, M. Ke, F. Zhang, and Z. Liu, *Nature (London)* **560**, 61 (2018).
- [22] K. J. A. Reijnders and M. I. Katsnelson, *Phys. Rev. B* **95**, 115310 (2017).
- [23] K. J. A. Reijnders and M. I. Katsnelson, *Phys. Rev. B* **96**, 045305 (2017).
- [24] B. Brun, N. Moreau, S. Somanchi, V.-H. Nguyen, K. Watanabe, T. Taniguchi, J.-C. Charlier, C. Stampfer, and B. Hackens, *Phys. Rev. B* **100**, 041401(R) (2019).
- [25] M.-H. Liu, C. Gorini, and K. Richter, *Phys. Rev. Lett.* **118**, 066801 (2017).
- [26] P. Bøggild, J. M. Caridad, C. Stampfer, G. Calogero, N. R. Papior, and M. Brandbyge, *Nat. Commun.* **8**, 15783 (2017).
- [27] C. Gutiérrez, L. Brown, C.-J. Kim, J. Park, and A. N. Pasupathy, *Nat. Phys.* **12**, 1069 (2016).
- [28] Y. Tan, M. M. Elahi, H.-Y. Tsao, K. Habib, N. S. Barker, and A. W. Ghosh, *Sci. Rep.* **7**, 1 (2017).
- [29] K. Wang, M. M. Elahi, L. Wang, K. M. Habib, T. Taniguchi, K. Watanabe, J. Hone, A. W. Ghosh, G.-H. Lee, and P. Kim, *Proc. Natl. Acad. Sci. U.S.A.* **116**, 6575 (2019).
- [30] Z. Li, T. Cao, M. Wu, and S. G. Louie, *Nano Lett.* **17**, 2280 (2017).
- [31] Y. Betancur-Ocampo, F. Leyvraz, and T. Stegmann, *Nano Lett.* **19**, 7760 (2019).
- [32] T. Ozawa, A. Amo, J. Bloch, and I. Carusotto, *Phys. Rev. A* **96**, 013813 (2017).
- [33] S. R. Zandbergen and M. J. A. de Dood, *Phys. Rev. Lett.* **104**, 043903 (2010).
- [34] M. C. Rechtsman, J. M. Zeuner, Y. Plotnik, Y. Lumer, D. Podolsky, F. Dreisow, S. Nolte, M. Segev, and A. Szameit, *Nature (London)* **496**, 196 (2013).
- [35] Y. Plotnik, M. C. Rechtsman, D. Song, M. Heinrich, J. M. Zeuner, S. Nolte, Y. Lumer, N. Malkova, J. Xu, A. Szameit *et al.*, *Nat. Mater.* **13**, 57 (2014).
- [36] L. Lu, J. D. Joannopoulos, and M. Soljačić, *Nat. Photonics* **8**, 821 (2014).
- [37] Y. Sun, D. Leykam, S. Nenni, D. Song, H. Chen, Y. D. Chong, and Z. Chen, *Phys. Rev. Lett.* **121**, 033904 (2018).
- [38] See Supplemental Material at <http://link.aps.org/supplemental/10.1103/PhysRevLett.129.233901> for more details on the experimental implementation of photonic graphene, on the description of the paraxial beam propagation, and discussions of the role of the barrier thickness

- and of the limit of the ordinary quantum-mechanical tunneling.
- [39] T. Ozawa, H. M. Price, A. Amo, N. Goldman, M. Hafezi, L. Lu, M. C. Rechtsman, D. Schuster, J. Simon, O. Zilberberg, and I. Carusotto, *Rev. Mod. Phys.* **91**, 015006 (2019).
- [40] F. D. M. Haldane and S. Raghu, *Phys. Rev. Lett.* **100**, 013904 (2008).
- [41] Z. Wang, Y. Chong, J. D. Joannopoulos, and M. Soljacic, *Nature (London)* **461**, 772 (2009).
- [42] M. Hafezi, S. Mittal, J. Fan, A. Migdall, and J. M. Taylor, *Nat. Photonics* **7**, 1001 (2013).
- [43] L.-H. Wu and X. Hu, *Phys. Rev. Lett.* **114**, 223901 (2015).
- [44] T. Ma, A. B. Khanikaev, S. H. Mousavi, and G. Shvets, *Phys. Rev. Lett.* **114**, 127401 (2015).
- [45] T. Ma and G. Shvets, *New J. Phys.* **18**, 025012 (2016).
- [46] L. Xu, H.-X. Wang, Y.-D. Xu, H.-Y. Chen, and J.-H. Jiang, *Opt. Express* **24**, 18059 (2016).
- [47] S. Barik, H. Miyake, W. DeGottardi, E. Waks, and M. Hafezi, *New J. Phys.* **18**, 113013 (2016).
- [48] F. Gao, H. Xue, Z. Yang, K. Lai, Y. Yu, X. Lin, Y. Chong, G. Shvets, and B. Zhang, *Nat. Phys.* **14**, 140 (2018).
- [49] F. Zhang, *Nat. Phys.* **14**, 111 (2018).
- [50] Z. Zhang, F. Li, G. Malpuech, Y. Zhang, O. Bleu, S. Koniakhin, C. Li, Y. Zhang, M. Xiao, and D. D. Solnyshkov, *Phys. Rev. Lett.* **122**, 233905 (2019).
- [51] Z. Zhang, S. Liang, F. Li, S. Ning, Y. Li, G. Malpuech, Y. Zhang, M. Xiao, and D. Solnyshkov, *Optica* **7**, 455 (2020).
- [52] Z. Zhang, R. Wang, Y. Zhang, Y. V. Kartashov, F. Li, H. Zhong, H. Guan, K. Gao, F. Li, Y. Zhang, and M. Xiao, *Nat. Commun.* **11**, 1902 (2020).
- [53] L. D. Landau and E. M. Lifshitz, *Quantum Mechanics: Non-Relativistic Theory* (Pergamon Press, Oxford, 1991).
- [54] L. L. Chang, L. Esaki, and R. Tsu, *Appl. Phys. Lett.* **24**, 593 (1974).
- [55] D. Solnyshkov, A. Nalitov, B. Teklu, L. Franck, and G. Malpuech, *Phys. Rev. B* **93**, 085404 (2016).
- [56] T. Jacqmin, I. Carusotto, I. Sagnes, M. Abbarchi, D. D. Solnyshkov, G. Malpuech, E. Galopin, A. Lemaître, J. Bloch, and A. Amo, *Phys. Rev. Lett.* **112**, 116402 (2014).
- [57] S. Klemmt, T. Harder, O. Egorov, K. Winkler, R. Ge, M. Bandres, M. Emmerling, L. Worschech, T. Liew, M. Segev *et al.*, *Nature (London)* **562**, 552 (2018).
- [58] D. Sanvitto and S. Kéna-Cohen, *Nat. Mater.* **15**, 1061 (2016).
- [59] B. Real, O. Jamadi, M. Milićević, N. Pernet, P. St-Jean, T. Ozawa, G. Montambaux, I. Sagnes, A. Lemaître, L. Le Gratiet *et al.*, *Phys. Rev. Lett.* **125**, 186601 (2020).